Shock Wave / Boundary Layer Interaction: A CFD Analysis of Shock Wave Propagation in Shock Tube Experiments

L.A. Oliveira*, L.R. Cancino, A.A.M. Oliveira
Combustion and Thermal Systems Engineering Laboratory - LABCET
Mechanical Engineering Department - EMC
Federal University of Santa Catarina - UFSC
Campus Universitario Trindade, Florianopolis, SC, 88040-900
Brazil

Key words: Shock wave/boundary layer interaction, CFD, Attenuation, Shock tube, Turbulence

Abstract:

Shock-tube experiments are used, among other applications, to analyze detailed chemical kinetics processes of practical fuels. In the low to intermediate temperature ignition range (700 k to 1100 K) are requires test times of the order of milliseconds. The test time available in practical devices is however limited /affected by several factors: (a) the arrival of the contact surface (b) the flow and thermodynamic conditions in the igniting mixture influenced by the growth of boundary layer, (c) the driven and driver sections length. This work presents the numerical results of the non-reactive shock waves propagation in shock tubes, by using computational fluid dynamic, as a tool to aid understanding the influence on boundary layer effects. The geometry for numerical simulations of the shock tube was adopted/proposed leaving into account realizable dimensions like internal diameter, driven and driver sections length. All simulations were performed assuming turbulent flow and using the Reynolds Stress Model in order to elucidate turbulent effects/influences. Also, the simulations were performed in order to achieve high pressure and low to intermediate temperature behind the reflected shock wave.

1. Introduction

The modern concept of shock wave and propagation of shock waves appears early in the 19^{th} century: "A shock wave is a surface of discontinuity propagating in a gas at which density and velocity experience abrupt changes. One can imagine two types of shock waves: (positive) compression shocks which propagate into the direction where the density of the gas is a minimum, and (negative) rarefaction waves which propagate into the direction of maximum density.". Zemplen (1905). Actually, not only on gases, shock wave effects have been observed in all four states of matter and also in media composed of multiple phases. It is now generally recognized that shock waves play a dominant role in most mechanical high-rate phenomena.

Shock waves can assume manifold geometry and exist in all proportions, ranging from the microscopic regime to cosmic dimensions. This has led to an avalanche of new shock-wave-related fields in physics, chemistry, materials science, engineering, military technology, medicine, among other research areas Krehl (2001). Specifically on fuel research, shock waves are used to analyze the chemical kinetics process of fuel ignition, by using shock tubes or high pressure shock tubes. One of the most important targets of shock tube experiments is the measurement of ignition delay time - IDT of reactive mixtures under engines like conditions, of this form, the mixture and thermodynamic conditions (stoichiometry, pressure and temperature) of the reactive mixture after the shocks are like internal combustion engines operation conditions. On shock tube experiments, the reactive mixture undergoes two pressure and temperature increases induced by the passage of incident and reflected shock waves respectively. The detailed operation of a shock tube have been explained in Cancino et al. (2009).

In an ideal shock tube, the incident and reflected waves propagates without any interaction with boundary layers, in a real case, the movement of incident waves generates a boundary layer around the tube wall and when the reflected shock wave come back, exist a strong interaction shock wave / boundary layer. This is a really important phenomenon and there is a big lack of information and literature about this process. In terms of incident wave / boundary layer interaction, Figure 1 (adapted from Mirels (1963)), presents a rendering of (a) the $x-t$ diagram and (b) the flow velocity profiles at time t_a for an incident shock wave. The difference between the ideal and the

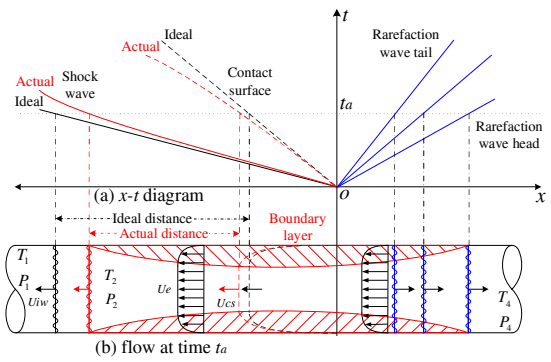

Figure 1. Boundary layer in shock tube (Adapted from Mirels (1963))

*Corresponding author: Mec.Eng. Leandro A. Oliveira, e-mail: leandroalves@labcet.ufsc.br

real positions of the shock and the contact surface can be noticed.

In figure 1, can be concluded that the presence of a wall boundary layer causes the shock to decelerate (shock attenuation), the contact surface to accelerate, and the flow to be non-uniform. Shock attenuation, in shock tube experiments is defined as the normalized slope of the axial velocity as extrapolated to the end wall (in %/meter), range for 1 to 4 %/m. The incident shock attenuation is due mainly to boundary layer buildup and non-ideal rupture of diaphragm Mirels (1963), Petersen and Hanson (2001).

Rudinger (1961) explain physically the effect of the boundary layer buildup: "As a result of boundary layer growth, the strength of the incident shock decreases as it propagates along the duct, but the pressure at a fixed location increases slightly with time."It means that attenuation of incident shock wave reflects in seriously consequences on the IDT measurements uncertainties, the reflected shock wave will meet the reactive mixture at a pressure level higher than the estimated by ideal shock relations, if pressure increase because boundary layer, the real pressure (and temperature) will be higher and subsequently, the thermodynamic conditions after reflected shock wave will be different when compared to the values estimated by ideal shock relations.

One small difference of 7 K in the conditions behind the incident wave will reflect on a difference of $\approx$ 50 K in the conditions behind the reflected shock wave, Cancino (2009). In chemical kinetics, a ΔT of 50 K can represent the ignitability of the reactive mixture, especially at low temperatures, high pressures and close or inside the Negative Temperature Coefficient - NTC behavior of straight hydrocarbons. This increase on pressure due to incident shock attenuation have been present in many experimental results reported in the literature, Cancino (2009), Petersen and Hanson (2001), Cancino et al. (2011), Lancheros et al. (2011), Cancino et al. (2010), Cancino et al. (2008). What have been done in order to overcome the uncertainties yields by the incident and reflected shock attenuation is the use of empirical/experimental correlations in order to "correct"the values of temperature, pressure and measured ignition delay times, as proposed by Petersen and Hanson (2001) and used by Cancino et al. (2010).

The focus of this work is to use a computational tool in order to understand and virtually visualize the shock wave / boundary layer interaction in shock tubes. This is the second work presented by the authors in this research area.

Next section will present the numerical models (simulation set-up). Section 3 will present the numerical results and some CFD visualization of the reflected shock wave / boundary layer interaction. Finally on section 4 are pointed out the main conclusions about the numerical approach of this work.

2. Numerical approach

2.1. Geometry and mesh

A shock tube is formed basically for two tubular sections, and assuming radial symmetry, the numerical simulation can be performed by using a full 2D axisymmetric geometry. For simulation purposes two shock-tube geometries were used: the first one (ST-G1), with driver and driven sections of 1.5 m and 2.0 m length, respectively and internal diameter is 60 mm. The geometry and meshes were generated by using the commercial ANSYS-FLUENT®Software. Figure 2 shows the geometric conception of the computational domain. Three computational mesh resolutions were

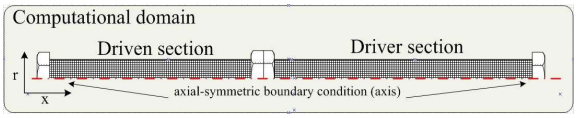

Figure 2. Shock tube - computational domain used in this work

used in this work, as shown in table 1. Three computational mesh resolutions were used in this work, details about mesh resolution and nodes number are shown in table 1. Note that, the mesh resolutions used in this work correspond (in percentage) to 75, 50 and 25% of the mesh resolutions used by Cancino et al. (2009). The second shock

Table 1. Mesh parameters for ST-G1

Parameter	mesh 1	mesh 2	mesh 3
Volumes	$1.85\text{x}10^{+6}$	$0.46\text{x}10^{+6}$	$0.21\text{x}10^{+6}$
Nodes	$1.86\text{x}10^{+6}$	$0.47\text{x}10^{+6}$	$0.21\text{x}10^{+6}$
Min. vol, m^3	$4.9\text{x}10^{-11}$	$6.2\text{x}10^{-8}$	$1.5\text{x}10^{-7}$
Ma.x vol, m^3	$1.4\text{x}10^{-8}$	$2.5\text{x}10^{-7}$	$5.6\text{x}10^{-7}$
Max. asp. ratio	4.772	3.841	3.505
Cell size, mm	0.25	0.5	0.75

tube geometry (ST-G2) mimics the real dimensions of the High Pressure Shock Tube at the University of Duisburg-Essen, Germany. The (ST-G2), presented schematically in Figure 2, has an internal diameter of 90 mm. It is separated by an aluminum diaphragm into a driver section of 6.1 m and a driven section of 6.4 m in length. The mesh resolution for (ST-G2) geometry was 0.25 mm. In order to obtain numerical data for reliable comparison process, the initial conditions and mixture set-up were assumed the same used by Cancino et al. (2009) that corresponds to real experimental conditions in shock tube experiments. Table 2 shows the values.

2.2. Numerical and turbulence models

Numerical simulations were preformed assuming transient, two dimensional, axisymmetric, compressible and turbulent flow, includding species transport without chemical reaction. The ANSYS-FLUENT®software employs finite-volume methods to numerically solve the discrete,

Table 2. Initial conditions and mixture set-up

Parameter	Value	Units
Ethanol/Air Equivalence ratio	1.0	
p_1	0.95	bar
T_1	325	K
Helium flux	200	Nm^3/h
Argon flux	16.8	Nm^3/h
Initial driver section pressure p_4	42	bar

coupled differential set of mass, energy, momentum and species transport conservation equations, as follows:

$$\partial\rho/\partial t + \nabla \bullet (\rho\overrightarrow{V}) = 0 \quad (1)$$

where ρ is density and $\overrightarrow{V}$ is the velocity, for momentum balance

$$\partial(\rho e)/\partial t + \nabla \bullet (\rho\overrightarrow{V} \times e) = \nabla(k_{effect}T) + \mu\Phi + S^{\phi} \quad (2)$$

where e is the total energy, k_{effect} is the effective thermal conductivity, T is the temperature, S^{ϕ} allows all the source terms, and $\mu\Phi$ are the viscid terms of energy equation. The selected materials were the pure substances, Argon and Helium, ethanol and air ANSYS-FLUENT®14.0 database. Species transport without chemical reaction was selected for mixtures, and then equations for transported species must be resolved for argon, helium, ethanol and molecular oxygen while molecular nitrogen (N_2) is computed by balance.

Thermal and full multicomponent diffusion were implemented with coefficients calculated internally in ANSYS-FLUENT ®by using kinetic theory. The simulations do not included fuel oxidation since the study is focused on fluid dynamic. The transient species transport equation can be formulated as

$$\partial(\rho\varphi_i)/\partial t + \nabla \bullet (\rho\overrightarrow{V} \times \varphi_i) = 0 \quad (3)$$

where φ_i is the concentration of the i chemical species. The turbulence model selected was Reynolds Stress Model (RSM), an second order turbulence modelling closes the Reynolds-Averaged Navier-Stokes (RANS) equations by solving additional transport equations for the six independent Reynolds stresses. Transport equations derived by Reynolds averaging is the result of the product of momentum equation with a fluctuating property. Closure model also requires one equation for turbulent dissipation.

The RSM have been used for accurately predicting complex flows and shows a good performane in shock wave propagation in shock tubes, Cancino et al. (2009). The RSM involves the modelling of turbulent diffusion (D_{ij}, D_{it}), pressure strain correlation (Ω_{ij}, Ω_{it}) which is the most involved part of the RSM, and the turbulent dissipation rate (ε_{ij}, ε_{it}). More details about RSM can be found in Pope (2000) and numerical inplementation in Ansys - Fluent (2011)

3. Numerical results

3.1. Incident / reflected shock attenuation

The numerical approach used in this work was able to capture the effect of the incident shock wave attenuation, in both the shock tube geometries simulated in this work. The pressure rise during the attenuation process is function, among other parameters like the internal diameter, for example, of the available time that is a direct function of the shock tube length.

It means that attenuation process could be easier to observe in larger shock tubes. Figure 3 shows the pressure rise as function of tube length (a) and time (b) for the ST-G2 geometry simulated in this work. Figure 3(a) shows the numeri-

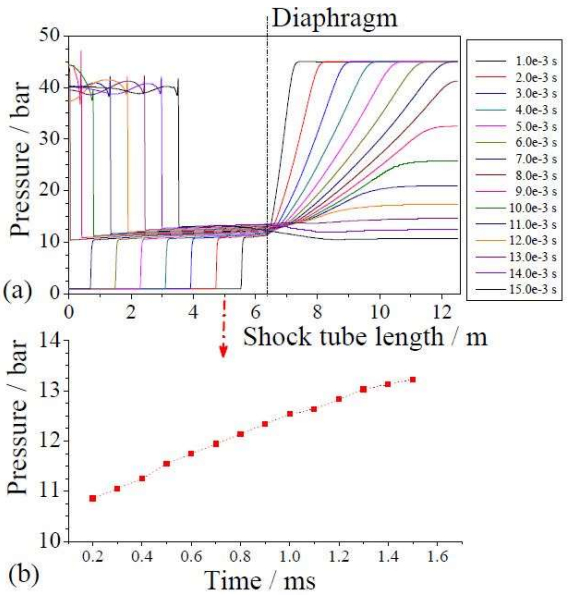

Figure 3. Pressure rise at $x = 5$ m from the end wall, due to incident shock attenuation - (ST-G2)

cal results of axial pressure distributions at several times, it can be observed the "movement" of the shock waves along the tube axis at several times. Figure 3(b) shows the pressure data (p_2) on several times, after the passage of the incident wave. One can observe that the pressure rises about 20 % in a short time of 1 ms.

This effect behind reflected shock waves have been experimentally observed an measured by several authors, Cancino (2009), Petersen and Hanson (2001), Davidson (2002), Lancheros et al. (2011), Cancino et al. (2010). In figure 3(a) can also be observed a slight pressure increase on time, at position $x = 0.5$ m from the end wall. The same effect of pressure rise was observed during the post-processing process of ST-G1 meshes 1 and 2, and not showed in this work.

3.2. Reflected shock wave / boundary layer interaction

As commented in section 1, there is a lack of information of reflected shock wave / boundary layer

interaction, even numerical and experiments. One of the focuses of this work is to numerically visualize and understand this process.

Figure 4 shows the location of the reflected shock wave, at flow time of 2.58x10^{-3} s. In this figure, (a), (b) and (c) shows the pressure, temperature and turbulence intensity respectively. In the left side is located the shock tube end wall, in this case a diameter of 60 mm, and one can see the reflected shock position approximately at $x = 85$ mm from the end wall. It can be observed that the

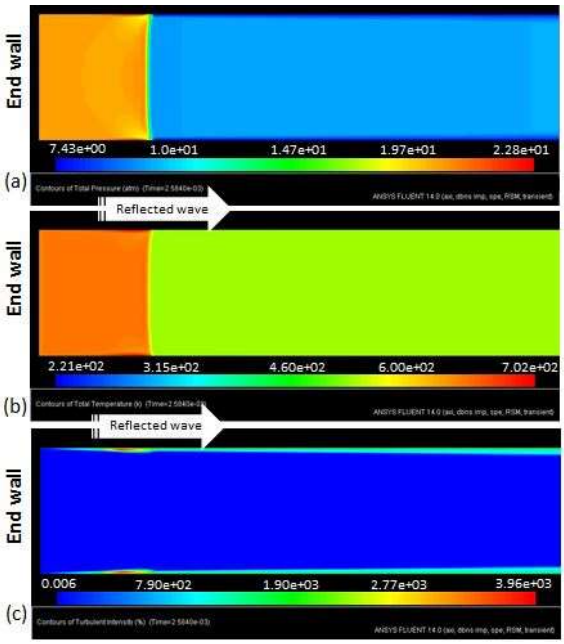

Figure 4. Flow at time 2.58x10^{-3} s. (ST-G1, mesh3)

shock wave is not completely plane, there is evident a curvature and a deformation of the shock wave near to the wall. These shape characteristics were also observed in the ST-G2 geometry, which diameter 30 % bigger that ST-G1 geometry.

Figure 5 shows the location of the reflected shock wave, at flow time of 2.7x10^{-3} s. In this figure, (a), (b) and (c) shows the pressure, temperature and turbulence intensity respectively. In the left side is located the shock tube end wall, in this case a diameter of 60 mm, and one can see the reflected shock position approximately at $x = 100$ mm from the end wall. Figure 6 shows the location of the reflected shock wave, at flow time of 2.96x10^{-3} s. In this figure, (a), (b) and (c) shows the pressure, temperature and turbulence intensity respectively. In the left side is located the shock tube end wall, in this case a diameter of 60 mm, and one can see the reflected shock position approximately at $x = 190$ mm from the end wall.

Several observations can be made from figures 4, 5 and 6. It can be noticed the increase of the thickness of the turbulent intensity layer, as result of the reflected shock wave propagation. In terms of IDT experiments, the gas-mixture behind the reflected shock is assumed to be quiescent. The fact of mixture movement close to the end wall

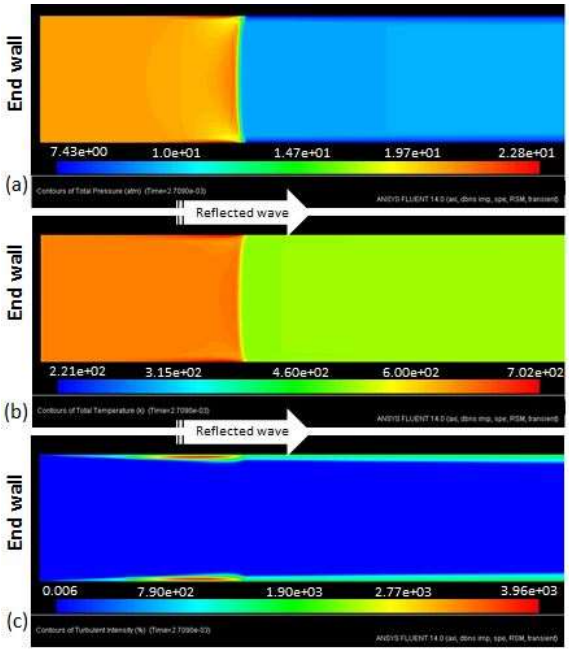

Figure 5. Flow at time 2.7x10^{-3} s. (ST-G1, mesh3)

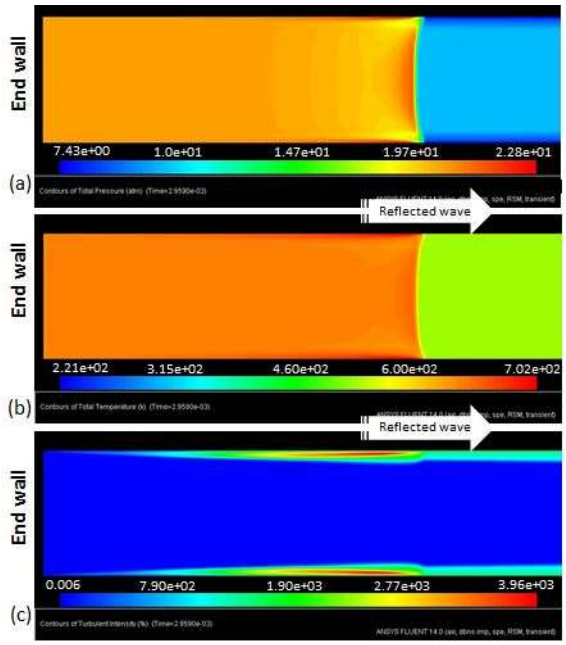

Figure 6. Flow at time 2.96x10^{-3} s. (ST-G1, mesh3)

can alter considerably the values, when compared to the numerically predicted by using detailed kinetics models for fuels ignition delay times.

The same behavior can be observed on pressure and temperature, considerable local fluctuation of the thermodynamics conditions are observed numerically, this because the mixture movement as result of turbulence, probably coming from the reflected shock wave / boundary layer interaction. Note that, this behavior was observed on both the ST-G1 and ST-G2 geometries (see figure 3(a)) for pressure fluctuations close to the shock tube end

wall.

Figure 7 shows the axial velocity, turbulent intensity and pressure distribution of a line a few millimeters behind the reflected shock wave. It can be observed the axial velocity inversion close to the tube wall, producing the adverse pressure gradient mentioned at literature, Zel'dovich et al. (1966), Zel'dovich et al. (1966b), Rudinger (1961), Mirels (1963). Also, it can be observed that this process happen very close to the tube wall (2.5 mm).

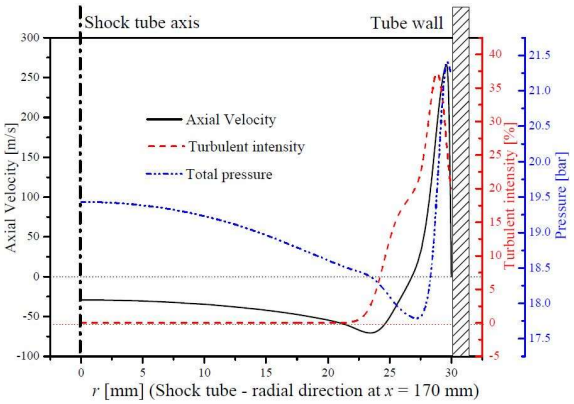

Figure 7. Axial velocity, Turbulent intensity and Pressure distributions in the radial direction at $x = 170$ mm. (ST-G1, mesh3)

Similar results were obtained for ST-G2, ST-G1 mesh1 and mesh2, however, the effect was observed to be more strong in the ST-G1 meshes (geometry with tube diameter of 60 mm), when compared to ST-G2 geometry, in agreement with literature Mirels (1963), Petersen and Hanson (2001).

4. Conclusions

4.1. About mesh resolution and computational time

Lower mesh resolution, adopted in order to more accurately capture the shock wave generates a serious problem in terms of computational time. Because the shock propagation is a transient simulation, the time-resolution for timing advancing must be very small. For ST-G1, meshes 1, 2 and 3, were necessary to use $0.2\text{x}10^{-7}$ s, $0.7\text{x}10^{-7}$ s and $1.0\text{x}10^{-6}$ s, as values of time step respectively.

It means that provably the direct numerical simulation of a propagating shock wave could be a non-practical process.

4.2. About the numerical approach

This work is an attempt to analyze by numerical simulation the propagating shock wave in a shock tube as an aid for the design and operation of shock tubes for chemical kinetic studies. Here, the structure of the compressible flow in a shock tube experiment was simulated for the conditions of the high-pressure shock-tube regular operation.

A stoichiometric mixture of ethanol / air was used as driven gas, and a helium / argon mixture as driver gases. Four structured meshes with 0.5, 0.75 and 0.25 mm of spatial resolution were used. The time discretization was variable, in agreement to the spatial resolution for convergence process. The Reynolds-Stress model was adopted in order to take into account the turbulent flow behind incident and reflected shock waves.

4.3. About reflected shock wave / boundary layer interaction

The RANS models captured the effect of the boundary layer growth behind the incident and reflected waves. Also, it was possible to capture the adverse pressure gradient tipically founded in shock wave / boundary layer interaction. Higher turbulence levels were located behind the contact surface in the core flow and behind the reflected shock wave near the walls, in both geometries and mesh resolution.

While temperatures behind incident and reflected shock waves are well predicted, the model failed to correctly predict the pressures, yielding errors of about 30-40%. Values of incident and reflected shock waves are in agreement with velocity predictions using one-dimensional shock relations.

Acknowledgements

The authors gratefully acknowledge the CNPq and ANP - Brazil, for the support given in the development of this work.

References

Ansys - Fluent 14 Documentation (2011). Ansys. Available at: http://www.ansys.com/

Cancino LR. Development and Application of Detailed Chemical Kinetics Mechanisms for Ethanol and Ethanol Containing Hydrocarbon Fuels. Ph.D thesis at Federal University of Santa Catarina, SC, Brazil. 2009.

Cancino LR, Oliveira AAM, Fikri M, Schulz C. Ignition delay times of ethanol-containing multi-component gasoline surrogates: shock-tube experiments and detailed modeling. Fuel (guildford), v. 90, p. 1238-1244, 2011.

Cancino LR, Oliveira AAM, Fikri M, Schulz C. Autoignition of gasoline surrogate mixtures at intermediate temperatures and high pressures: experimental and numerical approaches. Proceedings of the combustion institute, v. 32, p. 501-508, 2008.

Cancino LR, Oliveira AAM, Fikri M, Schulz C. Computational Fluid Dynamic Simulation of a Non-reactive Propagating Shock Wave in a Shock Tube. 27th International Symposium on Shock Waves - 19..24 July-2009, St. Petersburg.

Cancino LR, Oliveira AAM, Fikri M, Schulz C. Measurement and chemical kinetics modeling of shock-induced ignition of ethanol-air mixtures. Energy & Fuels, v. 24, p. 2830-2840, 2010.

Davidson DF, Oehlschlaeger MA, Herbon JT, Hanson RK, Shock tube measurements of iso-octane ignition times and OH concentration time histories, Proc. Comb. Inst. V29, 2002/pp. 1295-1301

Krehl P. Handbook of Shock Waves. Volume 1. Chap. 1 - History of Shock Waves, Pages 1-142. 2001. ISBN: 978-0-12-086430-0

Lancheros HPR, Fikri M, Cancino LR, Morac G, Schulz C, Dagaut P. Autoignition of surrogate biodiesel fuel (B30) at high pressures: experimental and modeling kinetic study. Combustion and Flame, v. 1, p. 1, 2011.

Mirels H. (1963). Test Time in Low-Pressure Shock Tubes., THE PHYSICS OF FLUIDS., Volume 6, Number 9.

Petersen EL, Hanson RK. Nonideal effects behind reflected shock waves in a high pressure shock tube. Shock Waves (2001) 10:405-420.

Pope SB. Turbulent Flows. Cambridge University Press. 2000.

Rudinger G. (1961). The Physics of Fluids., Volume 4, Number 12.

Zel'dovich YaB., Raizer YuP., Hayes WD., Probstein RF. (1966). Physics of Shock Waves and High-Temperature Hydrodynamic Phenomena. Volume I. ACADEMIC PRESS, New York and London.

Zel'dovich YaB., Raizer YuP., Hayes WD., Probstein RF. (1966). Physics of Shock Waves and High-Temperature Hydrodynamic Phenomena. Volume II. ACADEMIC PRESS, New York and London.

Zemplen G. University of Budapest. 1905. Hungary